



Article

Facile Synthesis of Iron-Titanate Nanocomposite as a Sustainable Material for Selective Amination of Substituted Nitro-Arenes

Manzar Sohail ¹, Nimra Tahir ¹, Anosha Rubab ¹, Matthias Beller ²  and Muhammad Sharif ^{3,*} 

¹ Department of Chemistry, School of Natural Sciences, National University of Sciences and Technology, Islamabad 44000, Pakistan; manzar.sohail@sns.nust.edu.pk (M.S.); ntahir.mschem18sns@student.nust.edu.pk (N.T.); arubab.mschem18sns@student.nust.edu.pk (A.R.)

² Leibniz-Institute for Catalysis e.V. an der Universitaet Rostock, Albert-Einstein-Strasse 29a, 18059 Rostock, Germany; Matthias.Beller@catalysis.de

³ Department of Chemistry, King Fahd University of Petroleum & Minerals, Dhahran 31261, Saudi Arabia

* Correspondence: msharif@kfupm.edu.sa; Tel.: +966-13-860-8725

Received: 2 July 2020; Accepted: 25 July 2020; Published: 3 August 2020



Abstract: The fabrication of durable and low-cost nanostructured materials remains important in chemical, biologic and medicinal applications. Particularly, iron-based nanomaterials are of central importance due to the ‘noble’ features of iron such as its high abundance, low cost and non-toxicity. Herein we report a simple sol–gel method for the synthesis of novel iron–titanium nanocomposite-based material ($\text{Fe}_9\text{TiO}_{15}@/\text{TiO}_2$). In order to prepare this material, we made a polymeric gel using ferrocene, titanium isopropoxide and THF precursors. The calcination of this gel in air at 500 °C produced Fe-Ti bimetallic nanoparticles-based composite and nano- TiO_2 as support. Noteworthy, our methodology provides an excellent control over composition, size and shape of the resulting nanoparticles. The resulted Fe-based material provides a sustainable catalyst for selective synthesis of anilines, which are key intermediates for the synthesis of several chemicals, dyes and materials, via reduction of structurally diverse and functionalized nitroarenes.

Keywords: iron titanate; sustainable catalysis; nanocomposites; nitroarenes; anilines; hydrogenation

1. Introduction

Among nanomaterials, synthesis of non-noble metal based nanostructures is crucial to mitigate the cost associated with the valued applications such as heterogeneous catalysis, biologic applications and many more [1,2]. Preparation of stable iron-based nanocomposite materials remains a foremost challenge for the advancement of chemical processes in academia, research in industrial processes and drug discovery [3–10]. Remarkably, more abundance, lesser price, environment friendly nature and less toxicity of iron make it an ideal element for many valuable applications. The high surface-to-volume ratio, low dimensionality, controllable particle size and morphology during synthetic processes, make them potential candidates for use in heterogeneous catalysis. Another key feature of iron nanoparticles as catalyst is magnetism of these materials, which allows effortless separation by an external magnet. Separation of catalyst by a magnet saves tedious and overwhelming processes of filtration and subsequently allowing the catalyst to be reused for multiple cycles [11]. Iron oxide nanoparticles appear in different morphologies depending upon the synthesis method and precursor salt being used. Hydrothermally stable iron oxide nanomaterials inherit water-tolerant property which make them desirable to be used for aqueous phase catalytic processes [12].

Considering the variable properties of iron nanoparticles, they have been employed in numerous applications ranging from nanocatalysis to biomedicine. In order to avoid agglomeration and volume

changes in iron oxide nanoparticles, support materials like activated carbon, silica, alumina and magnesium oxide have been incorporated for various organic transformations [13]. Iron based nanocatalysts have been widely known to serve the purpose in synthesis of hydrocarbons, not only by hydrogenation reaction of CO which is employed in Fischer-Tropsch process, but also through hydrogenation of CO₂ to prepare light olefins [14]. Ferrite nanocatalysts have been reported to be used in the treatment of waste water by oxidation process, allowing purification of water along with regeneration of adsorbed support surface [15]. Supported iron oxide nanoparticles as heterogeneous catalysts have been extensively investigated in a large number of processes such as acid-catalyzed reactions, C–C and C–O cross coupling reactions, oxidation and hydrogenation reactions [12]. Iron nanostructures have also been reported as anode materials for efficient and eco-friendly Li-ion batteries¹¹. Jagadeesh [16] et al. reported Fe₂O₃ support on nitrogen-doped graphene as a catalyst being explored for the synthesis of aromatic and aliphatic nitriles by employing NH₃ and O₂ as reactants, followed by catalytic hydrogenation of nitroarenes [17]. Cerium-doped iron titanite (FeCe_{0.3}Ti oxide) was employed for NO_x-reduction with NH₃ [18]. Iron-doped titania has also been used for a very challenging reduction of N₂ to NH₃ [19]. Very recently, iron oxide nanomaterials have emerged in various biologic applications such as, fabrication of bio sensors owing to their peroxidase-like activities¹¹, magnetic resonance and magnetic particle imaging contrast agents and in drug delivery as biocatalysts for nanotherapy [20].

Herein we report an expedient sol–gel process for the preparation of novel heterometallic iron and titanium (Fe₉TiO₁₅@TiO₂) nanocomposite material. Interestingly, this methodology leads to the formation of both Fe–Ti active nanoparticles and nano-TiO₂ as stable support. This new material is was tested for selective reduction of functionalized and structurally diverse nitroarenes to corresponding anilines using hydrazine hydrate as a source of hydrogen. Noteworthy, the resulting anilines constitute are key intermediate precursors for production of specialty and bulk chemicals, molecules significant in life sciences, dyes' industry and several petrochemicals.

2. Results and Discussion

2.1. Characterization of Fe₉TiO₁₅@TiO₂ Material

To investigate the structural features, we performed detailed characterization of Fe₉TiO₁₅@TiO₂ by powder X-ray diffraction (XRD), scanning electron microscopy (SEM), transmission electron microscopy (TEM), energy dispersive spectroscopy (EDS), X-ray photoelectron spectroscopy (XPS) and electron paramagnetic resonance (EPR). Figure 1 shows the XRD patterns of Fe₉TiO₁₅@TiO₂, Fe₉TiO₁₅, TiO₂ (anatase) and Fe₂O₃ (hematite). Fe₉TiO₁₅@TiO₂ is identified by JCPDS File no. 054–1267, with major peaks at 2θ = 33.16 (1 0 4), 35.64 (1 1 0), 54.08 (1 1 6), 62.44 (2 1 4) and 64.01° (3 0 0). Pure α-hematite prepared (by the calcination of ferrocene gel 500 °C, 4 h without Ti precursor) was identified by sharp reflection peaks in XRD. Similarly, pure anatase TiO₂ was obtained when only titanium isopropoxide gel was calcined (500 °C, 4 h). Broadening of XRD peaks in Fe₉TiO₁₅ is the evidence of successful doping of Ti⁴⁺ within the crystal lattice [21,22]. Here, TiO₂ is generated *in situ* and acts as the self-sacrificing support for iron-titania nanoparticles. TiO₂ produced is entirely in anatase phase, conclusively identified by major peaks at 2θ = 25.28° (1 0 1) and 48.05° (2 0 0) (JCPDS File no. 21–1272). The crystallite sizes by for Fe₉TiO₁₅ were estimated from XRD peaks by Debye–Scherrer method and were found to be in the range 11–18 nm.

Next, we performed SEM and TEM analysis to elucidate the size and distribution of nanoparticles, as well as the structure of Fe₉TiO₁₅@TiO₂. The SEM micrographs in Figure S1 show greatly porous nanostructures; EDX elemental mapping revealed that Fe and Ti metals were homogeneously dispersed and present in the each other's vicinity (Figure 2). TEM images at 100 nm resolution showed particles sized between 10–36 nm, which suggests that nanoparticles were constituted of 1–2 crystallites (Figure S2). Next, HRTEM images (Figure 3) showed that the nanoparticles were highly crystalline in nature and TiO₂ could be differentiated from Fe₉TiO₁₅ nanoparticles by measuring the inter planar distance from fringes as shown in Figure 3. The Fe₉TiO₁₅ particles possessed an interplanar distance

of 0.241 nm between well-defined fringes, while TiO_2 nanoparticles showed a 0.341-nm intra-fringe distance [22].

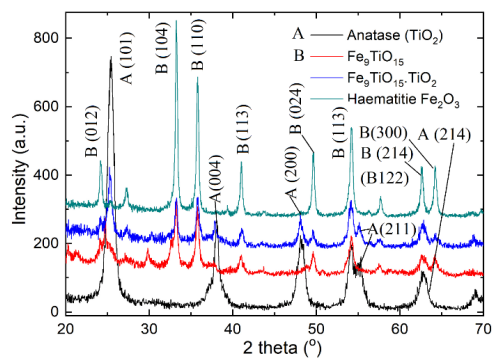


Figure 1. XRD patterns of $\text{Fe}_9\text{TiO}_{15}@TiO_2$ nanocomposites.

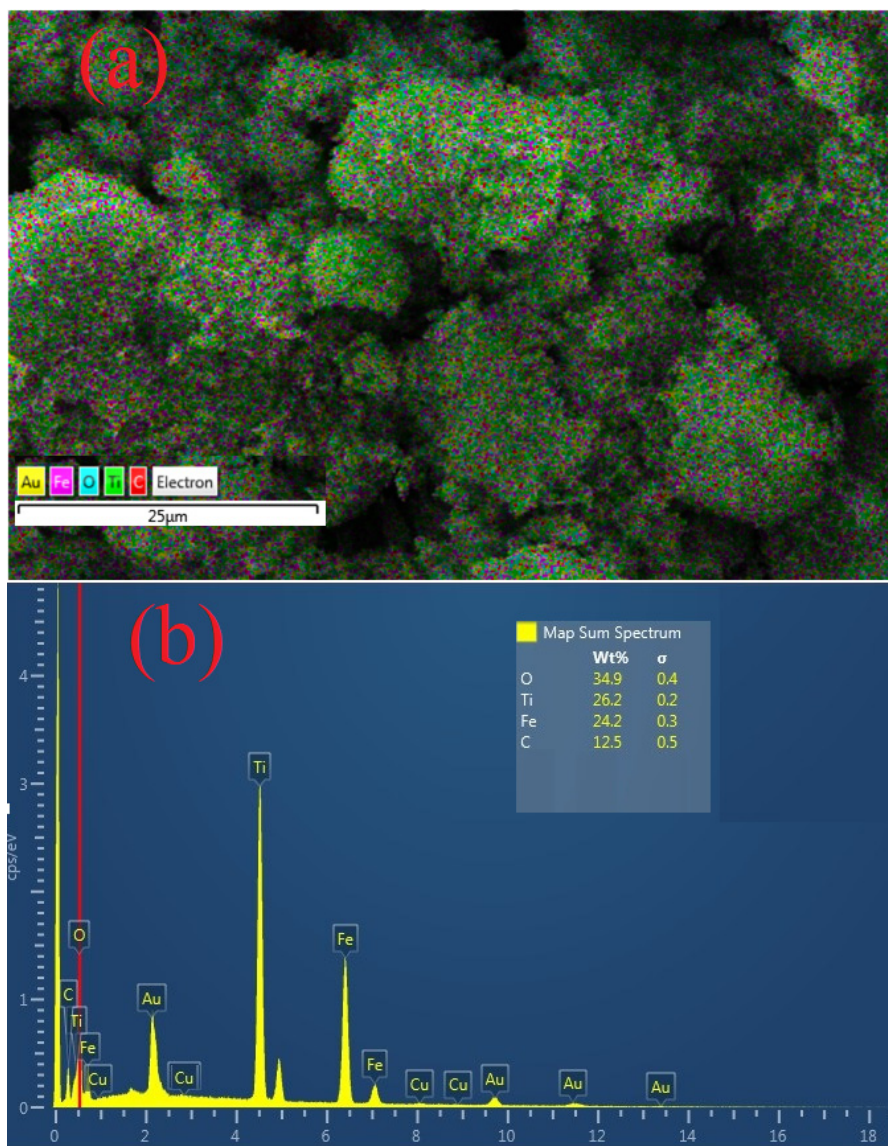


Figure 2. (a) Elemental mapping and (b) EDS spectrum of $\text{Fe}_9\text{TiO}_{15}\cdot\text{TiO}_2$.

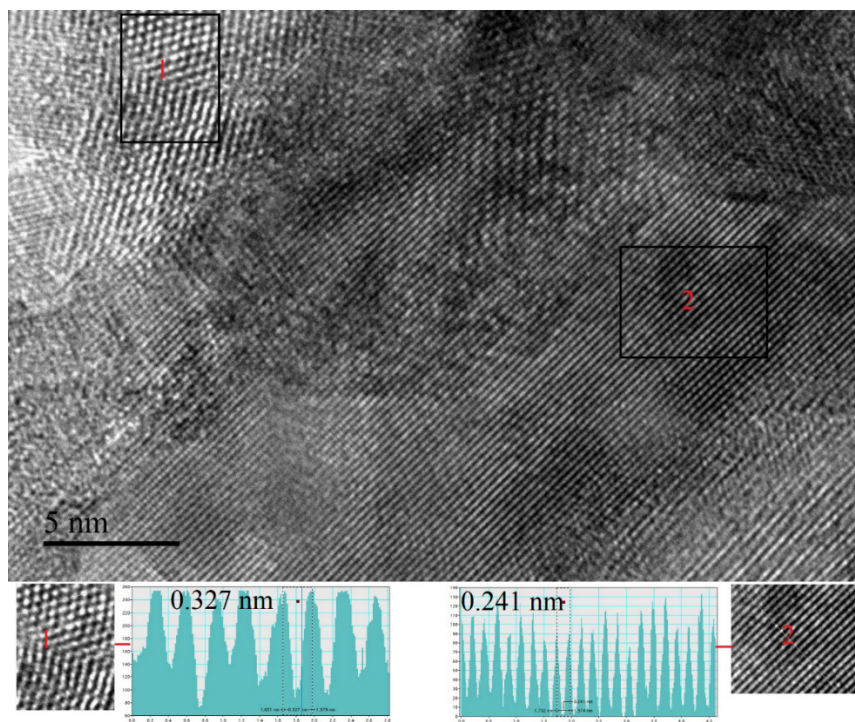


Figure 3. HRTEM image of $\text{Fe}_9\text{TiO}_{15}@\text{TiO}_2$ nanocomposite and IFFT analysis of the marked areas.

The XPS spectral analysis was performed to determine the elemental composition and oxidation states of iron and titanium (Figure 4). Peak fitting clearly showed the presence of both Fe(III) and Fe(II) species. A well resolved peak doublet at 710 eV ($2p_{3/2}$) and 723.9 eV ($2p_{1/2}$) represents Fe(II), while shoulder peaks due to presence of Fe(III) 2p peaks can be observed at 714.2 eV ($2p_{3/2}$) and 726.9 eV ($2p_{1/2}$) (Figure 4a) [23]. A predominant presence of Fe (II) may be due to the beam damage and electron gun used to compensate charging which can reduce Fe(III) to Fe(II) [24]. Ti (2p) XPS spectra (Figure 4b) shows that Ti(IV) specie present in titanium oxide. Typical sharp peaks of Ti($2p_{1/2}$) and Ti($2p_{3/2}$) are at 458.6 eV 464.3 eV. Respectively. The peak separation of 5.7 eV is assigned to titanium oxide. A satellite peak at 472.0 eV is also a feature of Ti (IV) in TiO_2 [21,23]. In addition, O(1s) XPS spectra shows the presence of two types of O atoms(Figure 4c); one at 530.0 eV and other 531.1 eV [21,23]. Both species lie in the typical metal oxide regions. Depending on the relative concentrations, first peak at 530.0 eV can be assigned to oxygen present in titanium oxide support and second peak at 531.1 eV can be assigned to oxygen atoms present in $\text{Fe}_9\text{TiO}_{15}$.

Further, EPR spectral analysis was performed (Figure 5) and found that the g-factor of $\text{Fe}_9\text{TiO}_{15}@\text{TiO}_2$ composite was found to be 2.19585. This is a normal value of Fe–complex systems and it is expected to be a bit higher than the free electron (2.002319) as it is correlated with the observed high oxidation state of the Fe species (+3). The broadness of signal is related to the presence of a Fe(II) atom present in the $\text{Fe}_9\text{TiO}_{15}$ [25,26]. All of these characterizations confirmed the formation of $\text{Fe}_9\text{TiO}_{15}$ bimetallic nanocomposite particles supported on in situ generated nano- TiO_2 support.

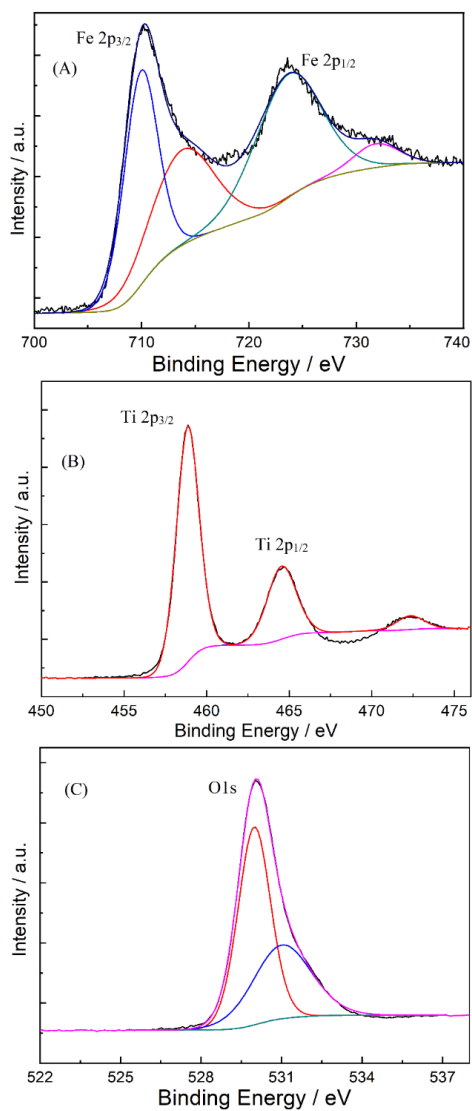


Figure 4. XPS spectra of Fe (2p) (A), Ti (2p) and (B) O (1s) (C) present in Fe₉TiO₁₅@TiO₂.

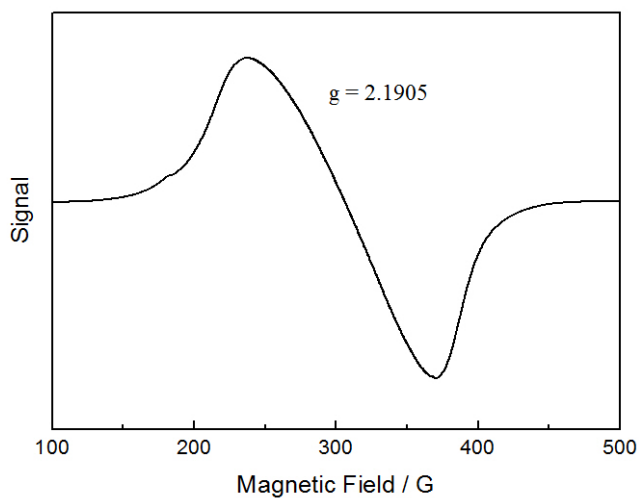
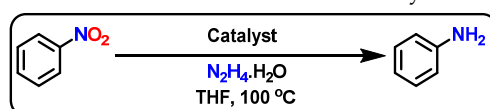


Figure 5. Electron paramagnetic resonance (EPR) spectra of Fe₉TiO₁₅@TiO₂.

2.2. Catalytic Applications of $\text{Fe}_9\text{TiO}_{15}@TiO_2$ for Selective Reduction of Nitroarenes to Anilines

Anilines represent central intermediates and key precursors for the synthesis of life science molecules, dyes, materials and petrochemical derivatives [27–33]. Generally, anilines have been prepared by the catalytic reduction or hydrogenation of nitroarenes [34,35]. Despite number of catalysts have been developed for this reaction [32,36–43], still the development of novel and selective nanocatalysts, especially based on iron is interesting. Here, we demonstrated the application of our prepared composite nanomaterial ($\text{Fe}_9\text{TiO}_{15}@TiO_2$) for the reduction of nitrobenzene as the model substrate using hydrazine hydrate as reducing agent. Hydrazine hydrate is an abundantly available inexpensive reagent and produces only water as a byproduct in reduction reactions [44]. It is commonly used as a reducing agent and hydrogen storage material, as well as a reagent in organic synthesis [44]. The reduction of nitrobenzene with $\text{Fe}_9\text{TiO}_{15}@TiO_2$ underwent complete conversion and produced aniline in high yields (Table 1; entry 1). Along with this material, we also tested newly prepared Fe_2O_3 and TiO_2 and found that these materials were not active. This clearly indicates that both the Fe or Ti particles alone are not active (Table 1, entries 2 and 3). However, bimetallic nanoparticles of Fe and Ti metals supported on nano- TiO_2 exhibits superior catalytic activity. As expected, the unpyrolyzed polymeric gel and catalyst under homogeneous conditions were also not active (Table 1; entries 4,5).

Table 1. Reduction of nitrobenzene: activity of catalysts.



Entry	Catalyst	Conversion (%)	Yield (%)
^a 1	$\text{Fe}_9\text{TiO}_{15}@TiO_2$	>99	99
^a 2	Fe_2O_3	<2	<1
^a 3	TiO_2	<2	<1
^a 4	Polymeric gel		
^b 5	Ferrocene + Titanium isopropoxide	<2	<1

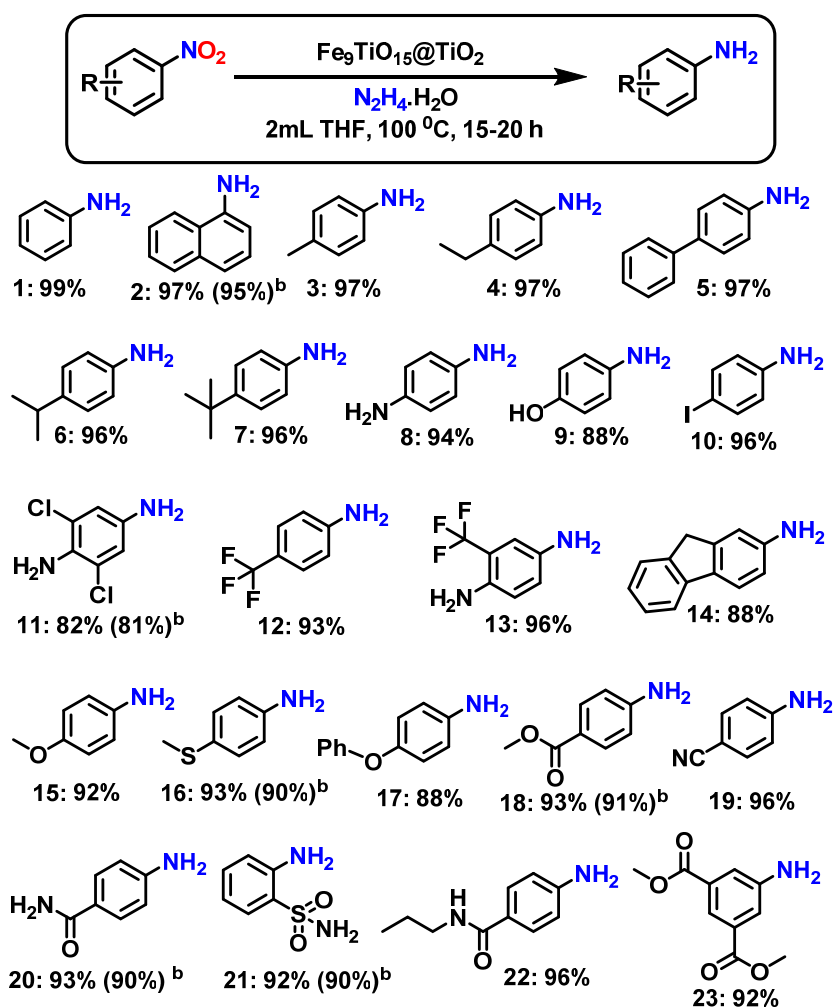
Reaction conditions: ^a 0.5-mmol nitroarene, 2.5-mmol hydrazine hydrate, 5 mg catalyst, 2 mL tetrahydrofuran (THF), 20, 100 °C. Yields were determined using n-hexadecane as standard. ^b Same as a with 0.02-mmol ferrocene and 0.03-mmol titanium isopropoxide. Fe_2O_3 was prepared using ferrocene. TiO_2 was prepared using titanium isopropoxide.

After having found the excellent activity of the $\text{Fe}_9\text{TiO}_{15}@TiO_2$ material, we demonstrated its general applicability for the reduction of nitro compounds. As shown in Schemes 1 and 2, structurally diverse and functionalized nitroarenes and heterocycles underwent highly selective reduction and produced corresponding aromatic and heterocyclic primary amines in good to excellent yields.

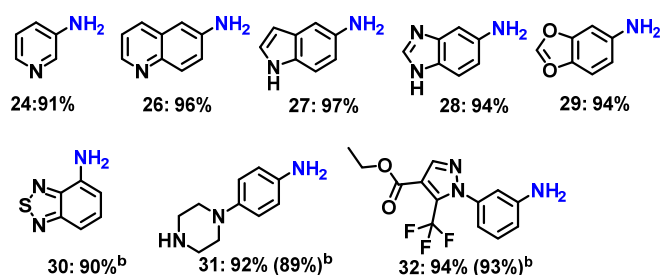
All the tested simple and substituted nitroarenes yielded respective anilines in up to 99% yields (Scheme 1; products 1–8). Interestingly, nitrophenol was reduced to aminophenol (88% yield; product 9), which is an important intermediate for the preparation of various dyes and pharmaceuticals; for example, paracetamol. Moreover, the presence of nitro-substituted phenols poses a major threat to vital human organs including kidneys, liver and central nervous system. Such nitrophenols are soluble in aqueous media and are not naturally degradable. In this regard, the present method offers suitable solution for the conversion of hazardous nitro phenol containing molecules to amino phenols [45]. Next, different halogenated anilines were obtained without being significant dehalogenation (Scheme 1; products 10–13). Importantly, iodo-nitrobenzene, which is more sensitive, is reduced to iodo-aniline without de-iodination (Scheme 1; product 10).

For demonstrating chemo-selectivity of our catalyst system, we tested various functionalized nitroarenes. Remarkably, the nitro was selectively reduced in presence of other reducible groups such as ether, thioether, ester, nitrile, amide and sulfonamide. Subsequently, we carried out the synthesis of amino-heterocycles (Scheme 2), which serve as important intimidates and starting materials for

various life science molecule as well as natural products. Here again, this Fe-based catalyst was highly active and selective for the reduction of nitro-heterocycles to amino-heterocycles in up to 97%.



Scheme 1. $\text{Fe}_9\text{TiO}_{15}@\text{TiO}_2$ nanocomposite catalyzed reduction of structurally diverse and functionalized nitroarenes to anilines. ^a Reaction conditions: 0.5-mmol nitroarene, 2.5-mmol hydrazine hydrate, 5 mg catalysts (4 mol% Fe), 2 mL THF, 15–20 h, 100 °C. Yields were determined using n-hexadecane as standard. ^b Scaled up by factor 4 and isolated yields are given.



Scheme 2. Selective reduction of heterocyclic nitro compounds to amino-heterocycles using $\text{Fe}_9\text{TiO}_{15}@\text{TiO}_2$ nanocatalysts. ^a Reaction conditions: 0.5-mmol nitroarene, 2.5-mmol hydrazine hydrate, 5 mg catalysts (4 mol% Fe), 2 mL THF, 15–20 h, 100 °C. Yields were determined using n-hexadecane as standard. ^b Scaled up by factor 4 and isolated yields are given.

Finally, we performed recycling of $\text{Fe}_9\text{TiO}_{15}@\text{TiO}_2$ catalyst for the reduction of nitrobenzene (Figure 6). Recycling and reusability of a given catalyst is an important aspects and crucial for the

advancement of cost-effective of chemical processes. Indeed, our catalyst was highly stable and reused up to 4 times without significant loss off activity and selectivity.

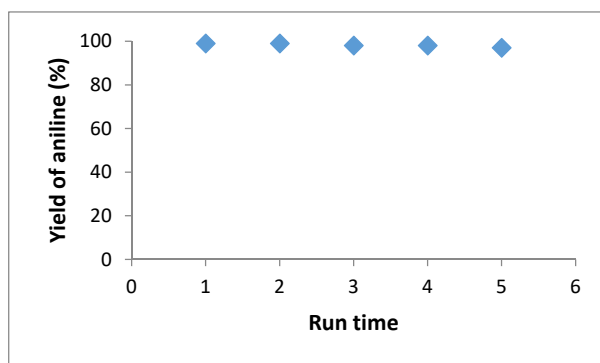


Figure 6. Recycling of $\text{Fe}_9\text{TiO}_{15}@/\text{TiO}_2$ catalysts for the reduction of nitrobenzene to aniline. Reaction conditions: 5-mmol nitrobenzene, hydrazine hydrate, 50 mg catalyst (4 mol% Fe), 20 mL THF, 15 h, 100 °C, yields were determined by GC using n-hexadecane as standard.

3. Experimental Section

3.1. Materials and Methods

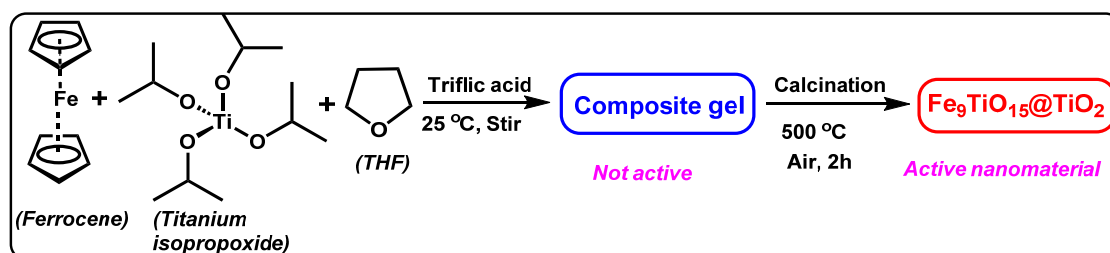
Ferrocene, titanium isopropoxide, triflic acid (TFC) and tetrahydrofuran (THF), nitro compounds and anilines were obtained from Sigma-Aldrich (Shanghai, China) and used without any purification. The XRD patterns were recorded using a Smart Lab X-ray diffractometer (Rigaku, Akishima-shi, Tokyo, Japan) using $\text{Cu-K}\alpha$ X-rays radiations ($\lambda = 0.15406$ nm). X-ray photoelectron spectroscopy (XPS) was carried out with ESCALAB 250Xi, Thermo Scientific Waltham, MA USA instrument. The adventitious carbon peak appeared at binding energy of 284.8 eV was used as a reference. The surface morphology (SEM) and energy dispersive X-ray (EDS), analysis were carried out by field emission scanning electron microscope (FESEM-Tescan Lyra-3, (Kohoutovice, Czech Republic) equipped with focused ion beam (FIB) and EDS, detector. TEM analysis were performed using scanning transmission electron microscope (FEI Tecnai F-20, Graz, Austria) coupled with a Fischione HAADF detector.

Electron paramagnetic resonance (EPR) spectra were recorded in X-band at 273 K on an Adani SPINSCAN X-band electron paramagnetic resonance (Minsk, Belarus) spectrometer equipped with Cavity Q factor and MW power measurement with a magnetic field modulation capability of 10 kHz–250 kHz. The data were measured at microwave frequency = 9.48 GHz; modulation amplitude = 8 G; modulation frequency = 100 kHz [46]. GC Conversion and yields were determined by GC-FID, HP6890 with FID detector, column HP530 m \times 250 mm \times 0.25 μm . NMR data were recorded on a Bruker ARX 300 and Bruker ARX 400 spectrometers. All catalytic reactions have been performed in pressure tubes purchased from Sigma-Aldrich. Pyrolysis and calcination was carried out in a Thermo Scientific Thermolyne industrial benchtop muffle furnace (Model 120 °C SSP) fitted with a has a B1 single-setpoint digital controller with ramp and dwell and 2.2 L heating area capacity, with a temperature range of 100–1200 °C.

3.2. Procedure for Preparation of $\text{Fe}_9\text{TiO}_{15}@/\text{TiO}_2$ Nanocomposite

In order to prepare Fe-Ti-based nanocomposites, first we mixed ferrocene and titanium isopropoxide in THF, then and initiated THF polymerization with the addition of few drops of TFC (Scheme 3 as reported recently by our research group [47,48]. In a 50-mL round bottomed flask, ferrocene (0.00537 M, 1 g) and titanium isopropoxide (0.0075 M, 2.13 g) were dissolved in 25 mL THF at room temperature. Then, a few drops of TFC were added for the polymerization of THF. Slow polymerization of THF was allowed to occur overnight with constant stirring at room temperature. After the formation of the polymeric gel, the entire reaction products were transferred to a crucible and

placed in furnace. Calcination was performed by raising the temperature to 500 °C at a rate of 4 °C per minute, then held for 2 h. After pyrolysis, the catalytic material was cooled to room temperature and stored in glass vials. ICP elemental analysis shows 22.8% of Fe and 25.6% of Ti, while EDX shows 24.2% of Fe and 26.2% of Ti. Elemental analysis results and EDX elemental mapping also shows similar results. Fe₉TiO₁₅ was prepared by using 9:1 molar ratios of the precursors (0.00537 M of ferrocene and 0.000596 M of titanium isopropoxide), TiO₂ (anatase) and Fe₂O₃ (hematite) were prepared under the similar conditions by using only titanium isopropoxide and ferrocene precursors, respectively.



Scheme 3. Synthesis of Fe-Ti nanocomposite material.

3.3. Procedure for Catalytic Reduction of Nitroarenes to Anilines

The procedure described earlier was followed [42]. The oven dried 25 mL ACE pressure autoclave vessel fitted with magnetic stir bar was charged with 0.5-mmol nitroarene in 2 mL THF. Then, 5 mg of Fe₉TiO₁₅@TiO₂ catalyst and 2.5-mmol hydrazine hydrate was added. Oxygen was removed from the reaction mixture by passing argon for 5 min. The pressure autoclave was then placed in the preheated aluminum block (100 °C) and left for 15–18 h at 100 °C. The autoclave tube was then removed from aluminum block and allowed to cool at room temperature. After autoclave was cooled down the cap was removed, and 100 µL hexadecane as internal standard was added. The catalyst was separated from the reaction mixture and GC-MS analysis of products was carried out. The corresponding aniline was purified by column chromatography (silica; n-hexane-ethyl acetate mixture), dried over anhydrous Na₂SO₄, solvent was removed in vacuum and NMR analysis of the product was carried out.

For recycling of the catalyst, a 5-mmol scale of reaction was carried out in a 50-mL pressure tube. After each run, the catalyst was washed with THF and ethyl acetate. The washed catalyst was in oven at 50 °C and reused for next run without any further purification.

4. Conclusions

New Fe-Ti-based nanocomposite materials (Fe₉TiO₁₅@TiO₂) were synthesized using simple sol-gel and calcination methodology. The generation of Fe-Ti polymeric gel using ferrocene, titanium isopropoxide and THF induced by triflic acid and subsequent calcination of this gel produced Fe₉TiO₁₅ bimetallic nanoparticles supported on nano-TiO₂. This new nanocomposite material revealed magnificent catalytic activity and selectivity for the production of functionalized and structurally diverse anilines from corresponding nitroarenes. The applicability, chemo-selectivity and recycling of this Fe-based nanomaterial was well-demonstrated.

Supplementary Materials: The following are available online at <http://www.mdpi.com/2073-4344/10/8/871/s1>, Representative ¹H- and ¹³C-NMR Spectra of Amines synthesized from nitroarenes are available as S1.

Author Contributions: M.S. (Manzar Sohail) and M.S. (Muhammad Sharif), and M.B.; contributed to the design of the project. M.S. (Manzar Sohail) and M.S. (Muhammad Sharif), N.T. and A.R.; contributed to the experiment and characterization. M.S. (Manzar Sohail), contributed to the drafting of the manuscript. M.B., provided scientific guidance, review, editing and consultation. M.S. (Muhammad Sharif); supervision, visualization, project administration, funding acquisition. All authors have read and agreed to the published version of the manuscript.

Funding: The research was supported by the Deanship of Scientific Research at the King Fahd University of Petroleum and Minerals, Dhahran, 31261, Kingdom of Saudi Arabia through project # DF191014.

Acknowledgments: The authors thank DSR at KFUPM for financial support through project # DF191014. The author acknowledge highly professional, kind and undoubted support of consultant in the project, H. C. Mult. Matthias Beller from Leibniz Institute for Catalysis Rostock, Germany.

Conflicts of Interest: The authors declare no conflicts of interest.

References

1. Wegener, S.L.; Marks, T.J.; Stair, P.C. Design Strategies for the Molecular Level Synthesis of Supported Catalysts. *Acc. Chem. Res.* **2012**, *45*, 206–214. [[CrossRef](#)] [[PubMed](#)]
2. Tieng, S.; Jia, Z.; Labidi, S.; Paola Diaz-Gomez Trevino, A.; Eloy, P.; Gaigneaux, E.M.; Chhor, K.; Kanaev, A. Major non-volatile intermediate products of photo-catalytic decomposition of ethylene. *J. Catal.* **2019**, *374*, 328–334. [[CrossRef](#)]
3. Jagadeesh, R.V.; Surkus, A.-E.; Junge, H.; Pohl, M.-M.; Radnik, J.; Rabeah, J.; Huan, H.; Schünemann, V.; Brückner, A.; Beller, M. Nanoscale Fe₂O₃-Based Catalysts for Selective Hydrogenation of Nitroarenes to Anilines. *Science* **2013**, *342*, 1073–1076. [[CrossRef](#)] [[PubMed](#)]
4. Murugesan, K.; Senthamarai, T.; Sohail, M.; Sharif, M.; Kalevaru, N.V.; Jagadeesh, R.V. Stable and reusable nanoscale Fe₂O₃-catalyzed aerobic oxidation process for the selective synthesis of nitriles and primary amides. *Green Chem.* **2018**, *20*, 266–273. [[CrossRef](#)]
5. Gawande, M.B.; Branco, P.S.; Varma, R.S. Nano-magnetite (Fe₃O₄) as a support for recyclable catalysts in the development of sustainable methodologies. *Chem. Soc. Rev.* **2013**, *42*, 3371–3393. [[CrossRef](#)]
6. Huber, D.L. Synthesis, Properties, and Applications of Iron Nanoparticles. *Small* **2005**, *1*, 482–501. [[CrossRef](#)]
7. Lee, N.; Yoo, D.; Ling, D.; Cho, M.H.; Hyeon, T.; Cheon, J. Iron Oxide Based Nanoparticles for Multimodal Imaging and Magnetoresponse Therapy. *Chem. Rev.* **2015**, *115*, 10637–10689. [[CrossRef](#)]
8. Chertok, B.; Moffat, B.A.; David, A.E.; Yu, F.; Bergemann, C.; Ross, B.D.; Yang, V.C. Iron Oxide Nanoparticles as a Drug Delivery Vehicle for MRI Monitored Magnetic Targeting of Brain Tumors. *Biomaterials* **2008**, *29*, 487–496. [[CrossRef](#)]
9. Torres Galvis, H.M.; Bitter, J.H.; Khare, C.B.; Ruitenbeek, M.; Dugulan, A.I.; de Jong, K.P. Supported Iron Nanoparticles as Catalysts for Sustainable Production of Lower Olefins. *Science* **2012**, *335*, 835. [[CrossRef](#)]
10. Shi, F.; Tse, M.K.; Pohl, M.M.; Brückner, A.; Zhang, S.; Beller, M. Tuning Catalytic Activity between Homogeneous and Heterogeneous Catalysis: Improved Activity and Selectivity of Free Nano-Fe₂O₃ in Selective Oxidations. *Angew. Chem. Int. Ed.* **2007**, *46*, 8866–8868. [[CrossRef](#)]
11. Lopez-Tejedor, D.; Benavente, R.; Palomo, J.M. Iron nanostructured catalysts: Design and applications. *Catal. Sci. Technol.* **2018**, *8*, 1754–1776. [[CrossRef](#)]
12. Rajabi, F.; Karimi, N.; Saidi, M.R.; Primo, A.; Varma, R.S.; Luque, R. Unprecedented selective oxidation of styrene derivatives using a supported iron oxide nanocatalyst in aqueous medium. *Adv. Synth. Catal.* **2012**, *354*, 1707–1711. [[CrossRef](#)]
13. Park, J.C.; Yeo, S.C.; Chun, D.H.; Lim, J.T.; Yang, J.-I.; Lee, H.-T.; Hong, S.; Lee, H.M.; Kim, C.S.; Jung, H. Highly activated K-doped iron carbide nanocatalysts designed by computational simulation for Fischer–Tropsch synthesis. *J. Mater. Chem. A* **2014**, *2*, 14371–14379. [[CrossRef](#)]
14. Wei, J.; Sun, J.; Wen, Z.; Fang, C.; Ge, Q.; Xu, H. New insights into the effect of sodium on Fe₃O₄-based nanocatalysts for CO₂ hydrogenation to light olefins. *Catal. Sci. Technol.* **2016**, *6*, 4786–4793. [[CrossRef](#)]
15. Bach, A.; Zelmanov, G.; Semiat, R. Cold catalytic recovery of loaded activated carbon using iron oxide-based nanoparticles. *Water Res.* **2008**, *42*, 163–168. [[CrossRef](#)]
16. Jagadeesh, R.V.; Junge, H.; Beller, M. Green synthesis of nitriles using non-noble metal oxides-based nanocatalysts. *Nat. Commun.* **2014**, *5*, 1–8. [[CrossRef](#)]
17. Jagadeesh, R.V.; Natte, K.; Junge, H.; Beller, M. Nitrogen-doped graphene-activated iron-oxide-based nanocatalysts for selective transfer hydrogenation of nitroarenes. *ACS Catal.* **2015**, *5*, 1526–1529. [[CrossRef](#)]
18. Zhang, W.; Shi, X.; Shan, Y.; Liu, J.; Xu, G.; Du, J.; Yan, Z.; Yu, Y.; He, H. Promotion effect of cerium doping on iron–titanium composite oxide catalysts for selective catalytic reduction of NO_x with NH₃. *Catal. Sci. Technol.* **2020**, *10*, 648–657. [[CrossRef](#)]
19. Wu, T.; Zhu, X.; Xing, Z.; Mou, S.; Li, C.; Qiao, Y.; Liu, Q.; Luo, Y.; Shi, X.; Zhang, Y.; et al. Greatly Improving Electrochemical N₂ Reduction over TiO₂ Nanoparticles by Iron Doping. *Angew. Chem. Int. Ed.* **2019**, *58*, 18449–18453. [[CrossRef](#)]

20. Wang, L.; Huo, M.; Chen, Y.; Shi, J. Iron-engineered mesoporous silica nanocatalyst with biodegradable and catalytic framework for tumor-specific therapy. *Biomaterials* **2018**, *163*, 1–13. [CrossRef]
21. Bickley, R.I.; Gonzalez-Carreno, T.; Gonzalez-Elipe, A.R.; Munuera, G.; Palmisano, L. Characterisation of iron/titanium oxide photocatalysts. Part 2.-Surface studies. *J. Chem. Soc. Faraday Trans.* **1994**, *90*, 2257–2264. [CrossRef]
22. Wu, W.-Q.; Lei, B.-X.; Rao, H.-S.; Xu, Y.-F.; Wang, Y.-F.; Su, C.-Y.; Kuang, D.-B. Hydrothermal Fabrication of Hierarchically Anatase TiO₂ Nanowire arrays on FTO Glass for Dye-sensitized Solar Cells. *Sci. Rep.* **2013**, *3*, 1352, Available online: <https://www.nature.com/articles/srep01352#supplementary-information> (accessed on 9 March 2019). [CrossRef] [PubMed]
23. Moulder, J.F.; Chastain, J. *Handbook of X-ray Photoelectron Spectroscopy: A Reference Book of Standard Spectra for Identification and Interpretation of XPS Data*. Electron Spectroscopy: Physical Electronics Division, Perkin-Elmer Corporation, 1995; Available online: <https://ci.nii.ac.jp/naid/10025039885/> (accessed on 28 July 2020).
24. Sohail, M.; De Marco, R.; Alam, M.T.; Pawlak, M.; Bakker, E. Transport and accumulation of ferrocene tagged poly (vinyl chloride) at the buried interfaces of plasticized membrane electrodes. *Analyst* **2013**, *138*, 4266–4269. [CrossRef] [PubMed]
25. McAlpin, J.G.; Surendranath, Y.; Dincă, M.; Stich, T.A.; Stoian, S.A.; Casey, W.H.; Nocera, D.G.; Britt, R.D. EPR Evidence for Co(IV) Species Produced During Water Oxidation at Neutral pH. *J. Am. Chem. Soc.* **2010**, *132*, 6882–6883. [CrossRef]
26. Mathies, G.; Chatziefthimiou, S.D.; Maganas, D.; Sanakis, Y.; Sottini, S.; Kyritsis, P.; Groenen, E.J.J. High-frequency EPR study of the high-spin FeII complex Fe[(SPPH₂)₂N]₂. *J. Magn. Reson. Imaging* **2012**, *224*, 94–100. [CrossRef]
27. Rappoport, Z. *The Chemistry of Anilines*; Wiley: Hoboken, NJ, USA, 2007.
28. Downing, R.S.; Kunkeler, P.J.; van Bekkum, H. Catalytic syntheses of aromatic amines. *Catal. Today* **1997**, *37*, 121–136. [CrossRef]
29. Ono, N. *The Nitro Group in Organic Synthesis*; John Wiley & Sons, Inc.: Bridgewater, NJ, USA, 2003; 1140 US Highway 22, East Suite, Bridgewater, NJ 08807 2002.
30. Sun, Z.; Bottari, G.; Barta, K. Supercritical methanol as solvent and carbon source in the catalytic conversion of 1,2-diaminobenzenes and 2-nitroanilines to benzimidazoles. *Green Chem.* **2015**, *17*, 5172–5181. [CrossRef]
31. Jagadeesh, R.V.; Banerjee, D.; Arockiam, P.B.; Junge, H.; Junge, K.; Pohl, M.-M.; Radnik, J.; Bruckner, A.; Beller, M. Highly selective transfer hydrogenation of functionalised nitroarenes using cobalt-based nanocatalysts. *Green Chem.* **2015**, *17*, 898–902. [CrossRef]
32. Westerhaus, F.A.; Jagadeesh, R.V.; Wienhöfer, G.; Pohl, M.-M.; Radnik, J.; Surkus, A.-E.; Rabeah, J.; Junge, K.; Junge, H.; Nielsen, M.; et al. Heterogenized cobalt oxide catalysts for nitroarene reduction by pyrolysis of molecularly defined complexes. *Nat. Chem.* **2013**, *5*, 537–543, Available online: <http://www.nature.com/nchem/journal/v5/n6/abs/nchem.1645.html#supplementary-information> (accessed on 3 May 2019). [CrossRef]
33. Corma, A.; Serna, P. Chemoselective Hydrogenation of Nitro Compounds with Supported Gold Catalysts. *Science* **2006**, *313*, 332. [CrossRef]
34. Wienhöfer, G.; Sorribes, I.; Boddien, A.; Westerhaus, F.; Junge, K.; Junge, H.; Llusar, R.; Beller, M. General and Selective Iron-Catalyzed Transfer Hydrogenation of Nitroarenes without Base. *J. Am. Chem. Soc.* **2011**, *133*, 12875–12879. [CrossRef] [PubMed]
35. Feng, J.; Handa, S.; Gallou, F.; Lipshutz Bruce, H. Safe and Selective Nitro Group Reductions Catalyzed by Sustainable and Recyclable Fe/ppm Pd Nanoparticles in Water at Room Temperature. *Angew. Chem. Int. Ed.* **2016**, *55*, 8979–8983. [CrossRef] [PubMed]
36. Blaser, H.-U.; Steiner, H.; Studer, M. Selective Catalytic Hydrogenation of Functionalized Nitroarenes: An Update. *ChemCatChem* **2009**, *1*, 210–221. [CrossRef]
37. Cantillo, D.; Baghbanzadeh, M.; Kappe, C.O. In Situ Generated Iron Oxide Nanocrystals as Efficient and Selective Catalysts for the Reduction of Nitroarenes using a Continuous Flow Method. *Angew. Chem. Int. Ed.* **2012**, *51*, 10190–10193. [CrossRef] [PubMed]
38. Shi, Q.; Lu, R.; Jin, K.; Zhang, Z.; Zhao, D. Simple and eco-friendly reduction of nitroarenes to the corresponding aromatic amines using polymer-supported hydrazine hydrate over iron oxide hydroxide catalyst. *Green Chem.* **2006**, *8*, 868–870. [CrossRef]

39. Rai, R.K.; Mahata, A.; Mukhopadhyay, S.; Gupta, S.; Li, P.-Z.; Nguyen, K.T.; Zhao, Y.; Pathak, B.; Singh, S.K. Room-Temperature Chemoselective Reduction of Nitro Groups Using Non-noble Metal Nanocatalysts in Water. *Inorg. Chem.* **2014**, *53*, 2904–2909. [[CrossRef](#)]
40. Singh, S.K.; Xu, Q. Nanocatalysts for hydrogen generation from hydrazine. *Catal. Sci. Technol.* **2013**, *3*, 1889–1900. [[CrossRef](#)]
41. Jagadeesh, R.V.; Wienhofer, G.; Westerhaus, F.A.; Surkus, A.-E.; Pohl, M.-M.; Junge, H.; Junge, K.; Beller, M. Efficient and highly selective iron-catalyzed reduction of nitroarenes. *Chem. Commun.* **2011**, *47*, 10972–10974. [[CrossRef](#)]
42. Sharma, U.; Kumar, P.; Kumar, N.; Kumar, V.; Singh, B. Highly Chemo- and Regioselective Reduction of Aromatic Nitro Compounds Catalyzed by Recyclable Copper(II) as well as Cobalt(II) Phthalocyanines. *Adv. Synth. Catal.* **2010**, *352*, 1834–1840. [[CrossRef](#)]
43. Ibele, M.E.; Wang, Y.; Kline, T.R.; Mallouk, T.E.; Sen, A. Hydrazine Fuels for Bimetallic Catalytic Microfluidic Pumping. *J. Am. Chem. Soc.* **2007**, *129*, 7762–7763. [[CrossRef](#)]
44. Kanaly, R.A.; Kim, I.S.; Hur, H.-G. Biotransformation of 3-Methyl-4-nitrophenol, a Main Product of the Insecticide Fenitrothion, by *Aspergillus niger*. *J. Agric. Food. Chem.* **2005**, *53*, 6426–6431. [[CrossRef](#)] [[PubMed](#)]
45. Bhowmik, T.; Kundu, M.K.; Barman, S. Ultra small gold nanoparticles-graphitic carbon nitride composite: An efficient catalyst for ultrafast reduction of 4-nitrophenol and removal of organic dyes from water. *Rsc Adv.* **2015**, *5*, 38760–38773. [[CrossRef](#)]
46. Pruckmayr, G.; Wu, T.K. Macrocyclic Tetrahydrofuran Oligomers. 2. Formation of Macrocycles in the Polymerization of Tetrahydrofuran with Triflic Acid. *Macromolecules* **1978**, *11*, 265–270. [[CrossRef](#)]
47. Sohail, M.; Sharif, M.; Khan, S.A.; Sher, M.; Jagadeesh, R.V. Method for the Synthesis of Nanoparticles of Heterometallic Nanocomposite Materials. U.S. Patent 1,045,020,1B2, 22 October 2019.
48. Sohail, M.; Baig, N.; Sher, M.; Jamil, R.; Altaf, M.; Akhtar, S.; Sharif, M. A Novel Tin-Doped Titanium Oxide Nanocomposite for Efficient Photo-Anodic Water Splitting. *ACS Omega* **2020**, *5*, 6405–6413. [[CrossRef](#)] [[PubMed](#)]



© 2020 by the authors. Licensee MDPI, Basel, Switzerland. This article is an open access article distributed under the terms and conditions of the Creative Commons Attribution (CC BY) license (<http://creativecommons.org/licenses/by/4.0/>).